

Fluctuating fractionalized spins in quasi-two-dimensional magnetic $V_{0.85}PS_3$

Vivek Kumar^{1,*}, Deepu Kumar¹, Birender Singh¹, Yuliia Shemerliuk², Mahdi Behnami,²
Bernd Büchner,^{2,3} Saicharan Aswartham² and Pradeep Kumar^{1,†}

¹*School of Basic Sciences, Indian Institute of Technology Mandi, Mandi-175005, India*

²*Leibniz-Institute for Solid-State and Materials Research, IFW-Dresden, 01069 Dresden, Germany*

³*Institute of Solid-State Physics, TU Dresden, 01069 Dresden, Germany*



(Received 25 June 2022; revised 4 February 2023; accepted 7 February 2023; published 15 March 2023)

Quantum spin liquid (QSL), a state characterized by exotic low energy fractionalized excitations and statistics, is still elusive experimentally and may be gauged via indirect experimental signatures. A remnant of the QSL phase may reflect in the spin dynamics as well as quanta of lattice vibrations, i.e., phonons, via the strong coupling of phonons with underlying fractionalized excitations. Inelastic light scattering (Raman) studies on $V_{1-x}PS_3$ single crystals evidence the spin fractionalization into Majorana fermions deep into the paramagnetic phase reflected in the emergence of a low frequency quasielastic response, along with a broad magnetic continuum marked by a crossover temperature $T^* \sim 200$ K from a pure paramagnetic state to a fractionalized spin regime qualitatively gauged via dynamic Raman susceptibility. We found further evidence of anomalies in the phonons' self-energy parameters, in particular, phonon line broadening and line asymmetry evolution at this crossover temperature, attributed to the decaying of phonons into itinerant Majorana fermions. This anomalous scattering response is thus indicative of fluctuating fractionalized spins suggesting a phase proximate to the quantum spin liquid state in this quasi-two-dimensional magnetic system.

DOI: [10.1103/PhysRevB.107.094417](https://doi.org/10.1103/PhysRevB.107.094417)

I. INTRODUCTION

The family of transition metal phosphorus trichalcogenides ($TMPX_3$, $TM = V, Mn, Fe, Co,$ or Zn and $X = S, Se$) with strong in-plane covalent bonds and a weak van der Waals gap between the layers of magnetic atoms has appeared as an intriguing candidate for exploring the quasi-two-dimensional (2D) magnetism, where the interplanar direct- and superexchange magnetic interactions are substantially quenched [1–3]. The underlying magnetic ground state ($|GS\rangle$) in these materials is affected by the trigonal distortion (TMX_6) due to change in the local symmetry from O_h to D_{3d} , which consequently lifts the degeneracy of the d orbitals. Magnetic studies on these materials reveals the emergence of a quite different magnetic $|GS\rangle$ on varying TM atoms, for example, $FePS_3$ shows an Ising-type transition at $T_N \sim 123$ K and $NiPS_3/MnPS_3$ undergoes a $XY/$ Heisenberg-type transition at $T_N = 155$ K/78 K [4]. We note that in this $TMPX_3$ family, vanadium-based systems remain largely unexplored beyond their basic properties. The recent reports on $V_{0.9}PS_3$ revealed an insulator to metal phase transition at a pressure of ~ 120 kbar without any structural transition and suggested a Kondo-type effect within the metallic phase. It was also advocated that this system lies in close proximity of the quantum spin liquid (QSL) state, a topologically active phase [1]. As the insulator to metal transition is also associated with the antiferromagnetic (AFM) to paramagnetic transition, it

opens the possibility of a highly entangled spin liquid phase due to a honeycomb lattice via potential Kitaev interactions. Interestingly, recently a new kind of Kondo behavior has been proposed and is attributed to gauge fluctuations from bond defects in spin liquids [5]. These experimental observations and theoretical predictions suggest a key route to the observation of the fascinating QSL state in these quasi-2D quantum magnetic materials. An important characteristic of these systems is that, despite all being isostructural, the magnetic lattice is a 2D honeycomb structure formed by TM ions, having different spin dimensionality. For example, the $|GS\rangle$ dynamics of the $MnPS_3$ member of this family is described by an isotropic ($J_{\perp} = J_{\parallel}$) Heisenberg Hamiltonian [$H = -\sum_{ij} J_{\perp}(S_{ix}S_{ix} + S_{iy}S_{iy}) + J_{\parallel}(S_{iz}S_{iz})$] and $FePS_3$ using the Ising ($J_{\perp} = 0$) model, whereas $NiPS_3$ is understood using the anisotropic ($J_{\perp} > J_{\parallel}$) model. This complexity is further enhanced in the $|GS\rangle$ of the V -based system $V_{0.85}PS_3$, also reflected in the magnetic measurements with $T_N \sim 60$ K, where the magnetic susceptibility exhibits intriguingly different behavior compared with other members of this family, suggesting the presence of an additional exotic competing interaction in the Hamiltonian, such as the Kitaev type, to completely understand the underlying magnetic $|GS\rangle$. We note that a similar behavior of χ_{mol} below T_N was also reported for $Cu_2Te_2O_5Br_2$ [6,7] which could be understood by quantum critical transition from the AFM state to the QSL state.

Signatures of the exotic $|GS\rangle$ in this system may emerge from the presence of strong quantum fluctuations due to entanglement of the underlying spins within the honeycomb lattice. Interest in the field of QSL was renewed with the seminal work of Kitaev in 2006 [8] and subsequently

*vivekvke@gmail.com

†pkumar@iitmandi.ac.in

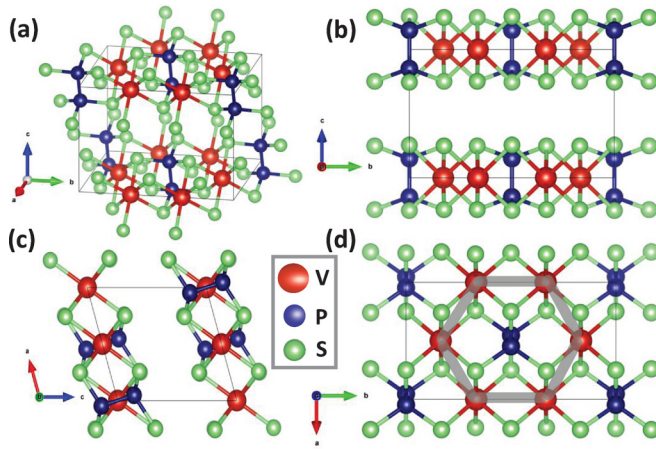


FIG. 1. Crystal structure of VPS_3 plotted using VESTA as viewed along (a) an arbitrary direction, (b) the a axis, (c) the b axis, and (d) the c axis; thick gray solid lines connecting the vanadium atoms represent a 2D honeycomb lattice formation. Red, blue, and green spheres represent vanadium, phosphorus, and sulphur, respectively.

certain conditions were laid down for the realization of a QSL state such as [9] the presence of a hexagonal honeycomb lattice, Mott insulator, edge-sharing octahedra in the structure, and spin-orbit coupling. A large number of systems have been proposed; however, so far there is not a single system which perfectly displays the QSL state as a true $|\text{GS}\rangle$, although numerous proposed systems do show a strong signature of a QSL state or a proximate QSL state [10–12]. However, in all those cases an ideal QSL state is preempted by long-range magnetic ordering at low temperature. Despite this, the signature of a QSL state may be captured as a fluctuation in the short-range ordering regime much before setting up of the long-range ordering. Recently, it was shown that a magnetic system, $\text{CrSi}/\text{GeTe}_3$, with $S = \frac{3}{2}$ and very weak spin-orbit coupling does reflect the signature of a QSL state understood using the $S = \frac{3}{2}$ XXZ -Kitaev model (represents the situation where exchange coupling is identical between the in-plane x -direction and y -direction but different along the out-of-plane z -direction) given as $H_{XXZ-K} = \sum_{\langle i,j \rangle} \frac{J_{\pm}}{2} (S_i^+ S_j^- + S_i^- S_j^+) + J_{\parallel} S_i^z S_j^z + K \sum_{\langle i,j \rangle \alpha} S_i^{\alpha} S_j^{\alpha}$ [13,14]. Also, the signature of fractionalized excitations was reported in a magnetic $S = \frac{1}{2}$ kagome AFM system attributed to a remnant QSL state [15]. In the case of a putative QSL candidate, $\alpha\text{-RuCl}_3$, it was shown that the low temperature zigzag AFM state is stabilized by quantum fluctuations with the spin liquid state as a proximate metastable state [16]. Generally, for a quantum spin liquid system frustration, dimerization, interchain/interlayer coupling, vacancy/defects leading to bond disorder, and spin-phonon coupling have an impact on the dynamics of the low energy excitations [6,17,18]. In 2D quantum systems, spin liquid $|\text{GS}\rangle$ or a remnant of the spin liquid phase is expected to be a consequence of exotic topologies, such as hexagonal honeycomb structure, as both the triangular and square lattice have AFM-like $|\text{GS}\rangle$ [6]. For $V_{1-x}\text{PS}_3$, we do have p - p dimer formation in the b - c plane (see Fig. 1), vacancy, and a hexagonal honeycomb lattice, hinting that it may have remnants of the QSL state as strong quantum fluctuations. Inherent coordination flexibility

and electronic configuration of the V ion makes it possible to realize exotic exchange with topologies.

Motivated by these suggestions and possibilities of a QSL state in these quasi-2D magnetic systems, we carried out an in-depth Raman scattering studies on a single crystal of $V_{0.85}\text{PS}_3$ (details of the synthesis are given in the Supplemental Material [19]; also see Refs. [1,20–33]) to understand the underlying exotic properties. Evidence of a QSL state or its remnant may be uncovered via observation of the quantum fluctuations of the associated spin degrees of freedom and their coupling with the lattice degrees of freedom through spin-phonon coupling. Inelastic light (Raman) scattering is an excellent technique to probe such dynamic quantum fluctuations reflected via the emergence of the quasielastic response at low energy and a broad continuum in the Raman response $\chi''(\omega, T)$ [34–38], smoking gun evidence of a QSL state. We note that the Raman signature of the QSL phase has been reported for different classes of materials. Sandilands *et al.* [39] reported Raman studies on $\alpha\text{-RuCl}_3$. Their measurements revealed unusual magnetic scattering typified by a broad continuum which survived until very high temperature (~ 100 K) as compared to the magnetic ordering temperature (~ 14 K) along with the phonon anomalies suggestive of frustrated magnetic interactions. They suggested that their observations may be understood using the combined Heisenberg-Kitaev model and advocated that $\alpha\text{-RuCl}_3$ may be close to a QSL ground state. A similar broad signature was also reported in other studies on $\alpha\text{-RuCl}_3$ and $\gamma\text{-Li}_2\text{IrO}_3$ [39–41]. Another class of putative QSL candidates is a spin $-\frac{1}{2}$ frustrated kagome compound called herbertsmithite, e.g., $\text{ZnCu}_3(\text{OH})_6\text{Cl}_2$. In these systems a similar broad continuum and phonon anomalies in the Raman spectroscopic as well as other optical measurements are identified with the possible fractionalized excitations associated with the QSL phase [41–45]. Another class of promising QSL candidates is the bis(ethylenedithio)tetrathiafulvalene (BEDT-TTF) molecule-based organic systems with highly frustrated triangular lattices [46–48]. We note that in these systems Raman as well as other optical techniques have been used to uncover the underlying QSL phase via observing a broad continuum and distinct in-gap excitations at low temperature and in the low energy regime.

Here for $V_{0.85}\text{PS}_3$, we observed a strong, low energy quasielastic response with lowering temperature and a broad continuum; quite startlingly, it starts emerging much above the long-range magnetic ordering temperature. These characteristic features clearly suggest the presence of strong underlying quantum fluctuations. Surprisingly, the corresponding amplitude of the estimated dynamic Raman susceptibility χ^{dyn} is not quenched below T_N , similar to the observed magnetic susceptibility, which is as expected for a conventionally ordered system, signaling that it emerges from a proximate QSL state or its remnant. Our observations evince the signature of a remnant QSL state as a fluctuating part suggest that this system lies in the proximity of a QSL ground state. This also suggests that the low temperature ordered phase may be proximate to the quantum phase transition into a spin liquid $|\text{GS}\rangle$. The anomalies observed in the χ^{dyn} maps are parallel with the anomalies seen in the self-energy parameters of the phonon modes, i.e., peak frequencies and linewidths. Here, we

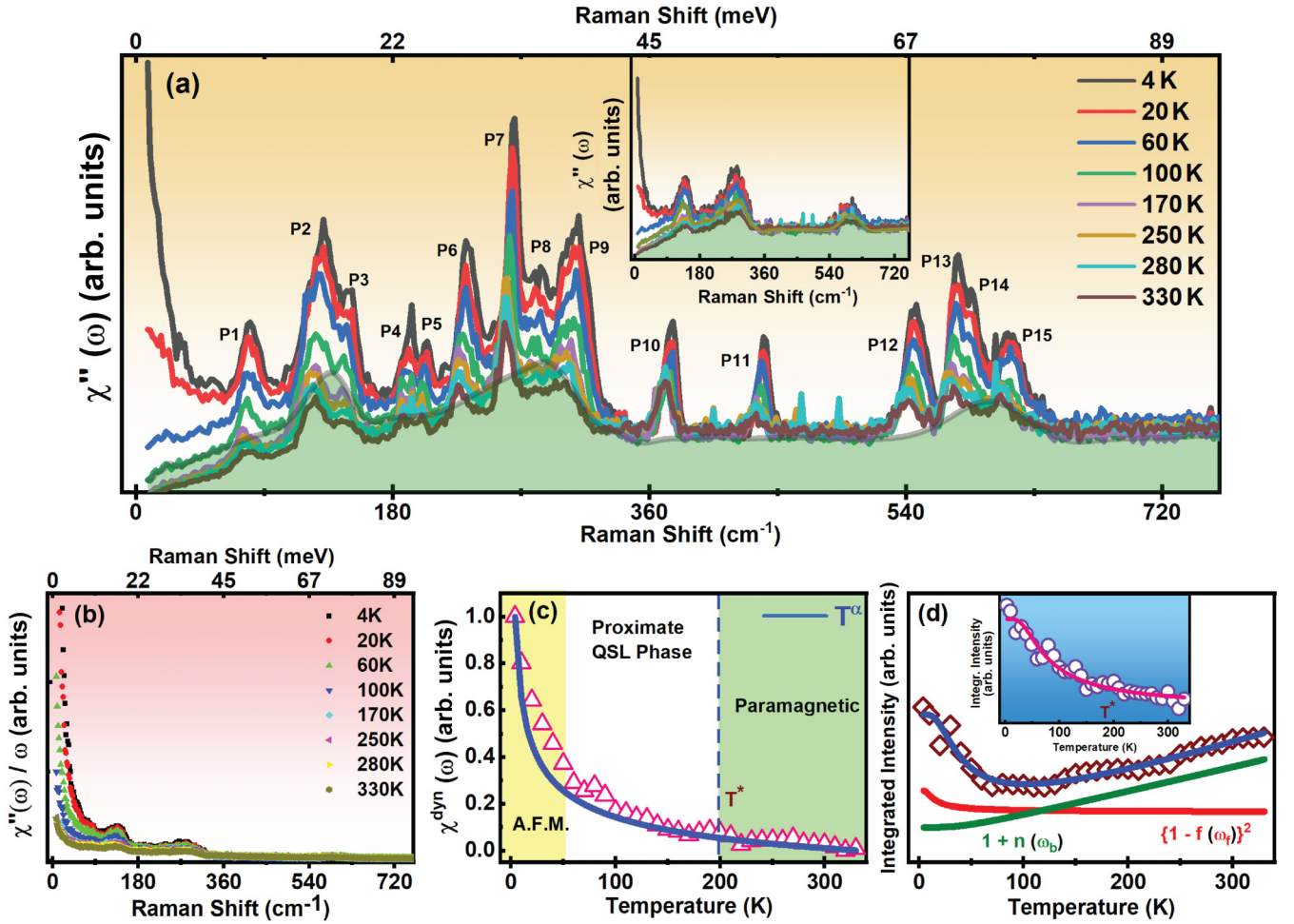


FIG. 2. (a) Temperature evolution of the Raman response $\chi''(\omega, T)$ [measured raw Raman intensity/ $1 + n(\omega, T)$]. The inset shows the phonons' subtracted Raman response. Labels P1 – P15 represent phonon modes. (b) Temperature dependence of the phonons' subtracted Raman conductivity $\chi''(\omega, T)/\omega$. (c) Temperature dependence of $\chi''^{\text{dyn}}(T)$ obtained from the Kramers-Kronig relation. The solid blue line is the power-law fit $\chi''^{\text{dyn}} \sim T^\alpha$. Background colored shading reflects different magnetic phases. (d) The main panel shows integrated raw spectra intensity in the energy range 1 – 95 meV; the blue solid line shows fitting by a combined bosonic and fermionic function, $[a + b\{1 + n(\omega_b, T)\}] + c\{1 - f(\omega_f, T)\}^2$. Solid green and red lines show temperature dependence of bosonic and fermionic function. The inset shows the magnetic contribution to the Bose-corrected integrated intensity and T^* (~ 200 K) represents the temperature where spin fractionalization starts building up. The pink solid line represents fitting by the two-fermion scattering function $a + b[1 - f(\omega, T)]^2$, where $f(\omega, T) = 1/[1 + e^{\hbar\omega_f/k_B T}]$ is the Fermi distribution function.

report the experimental evidence supporting the existence of a remnant QSL phase in $V_{0.85}PS_3$ using Raman spectroscopy.

II. RESULTS AND DISCUSSION

A. Temperature evolution of the broad magnetic continuum

Magnetic Raman scattering gives rise to a broad continuum originating from underlying dynamical spin fluctuations and may be used to gauge the fractionalization of quantum spins expected for proximate spin liquid candidates [39,41,49–54]. To investigate the possible emergence of the fermionic excitations, we carried out a detailed analysis of the temperature evolution of the observed broad magnetic continuum in the Raman spectra. The fractional spin excitations play a key role in dictating the temperature evolution of the background continuum of the Raman spectra because their occupation is determined by the Fermi distribution function. First, we

focus on the temperature evolution of the integrated intensity of the background continuum to determine the fractionalized excitations' energy scale [53], where the raw Raman intensity $I(\omega)$ is integrated over a range of 1.0 – 95 meV as $I = \int_{\omega_{\text{min}}}^{\omega_{\text{max}}} I(\omega, T) d\omega$. Figure 2(d) shows the temperature evolution of the integrated intensity of the background continuum. As can be seen from Fig. 2(d), the integrated intensity of the background continuum shows a nonmonotonic temperature dependence; at high temperature the intensity variation is mainly dominated by a conventional one-particle scattering corresponding to the thermal Bose factor given as $I(\omega, T) \propto [1 + n(\omega, T)]$, where $[1 + n(\omega, T)] = 1/[1 - e^{-\hbar\omega_b/k_B T}]$. However, at low temperature a significant deviation from the conventional bosonic excitations is observed below ~ 150 K; the intensity shows a monotonic increase with decreasing temperature down to the lowest recorded temperature (4 K). To understand the temperature dependence

of the integrated intensity of the background continuum, we fitted it with a function having contributions from both bosonic and two-fermion (related to the creation and annihilation of the pair of fermions, its functional form is given as $a + b[1 - f(\omega, T)]^2$, where $f(\omega, T) = 1/[1 + e^{\hbar\omega_f/k_B T}]$ is the Fermi distribution function with zero chemical potential [53]) excitations. The fitting outcome reveals that the temperature dependence of the integrated intensity below ~ 150 K is mainly dominated by fermionic excitations and the corresponding fractionalized energy scale for the fermions is $\omega_f = 10.3$ meV (~ 85 cm $^{-1}$). The temperature evolution of the integrated intensity of Bose-corrected spectra is shown in the inset of Fig. 2(d), clearly indicating the significant enhancement of the magnetic contribution below ~ 150 – 200 K as fitting well with the two-fermion function, $a + b[1 - f(\omega, T)]^2$. Our analysis suggests the signature of fractionalized fermionic excitations in $V_{0.85}\text{PS}_3$, a key signature of the proximate QSL phase, in line with the other 2D honeycomb putative QSL candidates, α - RuCl_3 as well as Li_2IrO_3 [39,41]. In a conventional long range ordered magnetic system, the background continuum develops into relatively sharp modes (magnons with spin -1) below T_N [55]. We note that in other members of this family, e.g., for FePS_3 , additional low frequency (below ~ 150 cm $^{-1}$) sharp modes were observed below T_N , attributed to the magnetic excitations [56]. On the other hand, we did not observe any such sharp peaks below T_N , or development of the broad underlying continuum into sharp modes; additionally, we observed Fano line asymmetry and phonon anomalies in line with the theoretical suggestion for phonons in putative QSL candidates. Also, we observed that the quasielastic response increases with decreasing temperature; on the other hand in case of a conventional magnetic system quasielastic response increases with increasing temperature due to thermal fluctuations.

Now we will discuss the Raman response, $\chi''(\omega, T)$, which shows the underlying dynamic collective excitations at a given temperature, where $\chi''(\omega, T)$ is calculated by dividing raw Raman intensity with the Bose factor, $I(\omega, T) \propto [1 + n(\omega, T)]\chi''(\omega, T)$. The Raman response, $\chi''(\omega, T)$, is proportional to Stokes Raman intensity given as $I(\omega, T) = \int_0^\infty dt e^{i\omega t} \langle R(t)R(0) \rangle \propto [1 + n(\omega, T)]\chi''(\omega, T)$, where $R(t)$ is the Raman operator and $[1 + n(\omega, T)]$ is the Bose thermal factor. Figure 2(a) shows the temperature evolution of $\chi''(\omega, T)$. We note that $\chi''(\omega, T)$ is composed of the phononic excitations superimposed on a broad continuum extending up to ~ 95 meV. The detailed analysis of the self-energy parameters of all the observed phonon modes; i.e., peak frequency and linewidth, is given in the Appendix. An in-depth analysis of this broad continuum may provide further information about the underlying nature of the dynamical spin fluctuations via the dynamic Raman susceptibility (χ^{dyn}). Interestingly the Raman response shows a significant increase in the spectral weight on lowering the temperature [see Fig. 2(a) and its inset], and quite surprisingly it continues to increase upon entering into the spin-solid phase unlike the conventional systems where it is expected to quench below T_N . This characteristic scattering feature is typical of the scattering from underlying quantum spin fluctuations. For further probing the evolution of this broad magnetic continuum and underlying quantum spin fluctuations we

quantitatively evaluated χ^{dyn} , shown in Fig. 2(c). χ^{dyn} at a given temperature is evaluated by integrating the phonon subtracted Raman conductivity, $\chi''(\omega)/\omega$, shown in Fig. 2(b), and using the Kramers-Kronig relation as

$$\chi^{\text{dyn}} = \lim_{\omega \rightarrow 0} \chi(k=0, \omega) \equiv \frac{2}{\pi} \int_0^\Omega \frac{\chi''(\omega)}{\omega} d\omega, \quad (1)$$

where Ω is the upper cutoff value of the integrated frequency chosen as ~ 95 meV, where Raman conductivity shows no change with further increase in the frequency. With lowering temperature χ^{dyn} shows nearly temperature-independent behavior down to ~ 200 K as expected in a pure paramagnetic phase; on further lowering the temperature it increases continuously until 4 K. The relative change in the temperature range of 330–200 K increases only by $\sim 19\%$, at 200–60 K it increases by $\sim 73\%$, and there is a 126% increase in the 60–4 K range. In the quantum spin liquid phase, the Raman operator couples to the dispersing fractionalized quasiparticle excitation and reflects the two Majorana fermion density of states [51]. Therefore, an increase in the χ^{dyn} below ~ 200 K reflects the enhancement of the Majorana fermion density of states and marks the crossover from a paramagnetic to the proximate spin liquid state. Remarkably, the temperature dependence of the phonon modes also showed the anomalies around ~ 200 K, reflecting the strong coupling of fractionalized excitations with the lattice degrees of freedom (discussed in Sec. II B below). For conventional antiferromagnets as the system attains ordered phase the dynamical fluctuations should be quenched to zero; contrary to that here we observed a significant increase in dynamic Raman susceptibility hinting at strong enhancement of dynamic quantum fluctuations [6,54,57,58]. The diverging nature of $\chi^{\text{dyn}}(T)$ as $T \rightarrow 0$ K clearly suggests the dominating nature of quantum fluctuations associated with the underlying collective excitations down to the lowest temperature. This is also consistent with recent theoretical understanding, where it was advocated that dynamic correlations may have unique temperature dependence in systems with quantum spin liquid signatures and the fractionalization of the quantum spins contributes to dynamic spin fluctuations even in the high temperature paramagnetic phase [59]. Therefore, naturally the signature of spin fractionalization is expected to be visible in the dynamical measurable properties such as dynamic Raman susceptibility as observed here. It was also shown that in the low temperature regime the dynamical structure factor, related with the spin-spin correlation function, shows a quasielastic response with lowering temperature and was suggested as evidence for fractionalization of spins.

Next, we focus on the very low frequency region (LFR), i.e., 1–9 meV, where we observed the emergence of a strong quasielastic response at low temperature; see Figs. 3(a) and 3(b). We evaluated the dynamic Raman susceptibility $\chi_{\text{LFR}}^{\text{dyn}}$ for this low energy range [see Fig. 3(c)]. The observed $\chi_{\text{LFR}}^{\text{dyn}}$ remains nearly constant until ~ 200 K, and shows a monotonic increase with further decreasing the temperature down to 4 K. We fitted both χ^{dyn} and $\chi_{\text{LFR}}^{\text{dyn}}$ using a power law as $\chi^{\text{dyn}} \sim T^\alpha$ ($\alpha = -0.34$ for χ^{dyn} [see the solid blue line in Fig. 2(c)] and $\alpha = -0.67$ for $\chi_{\text{LFR}}^{\text{dyn}}$ [see the solid line

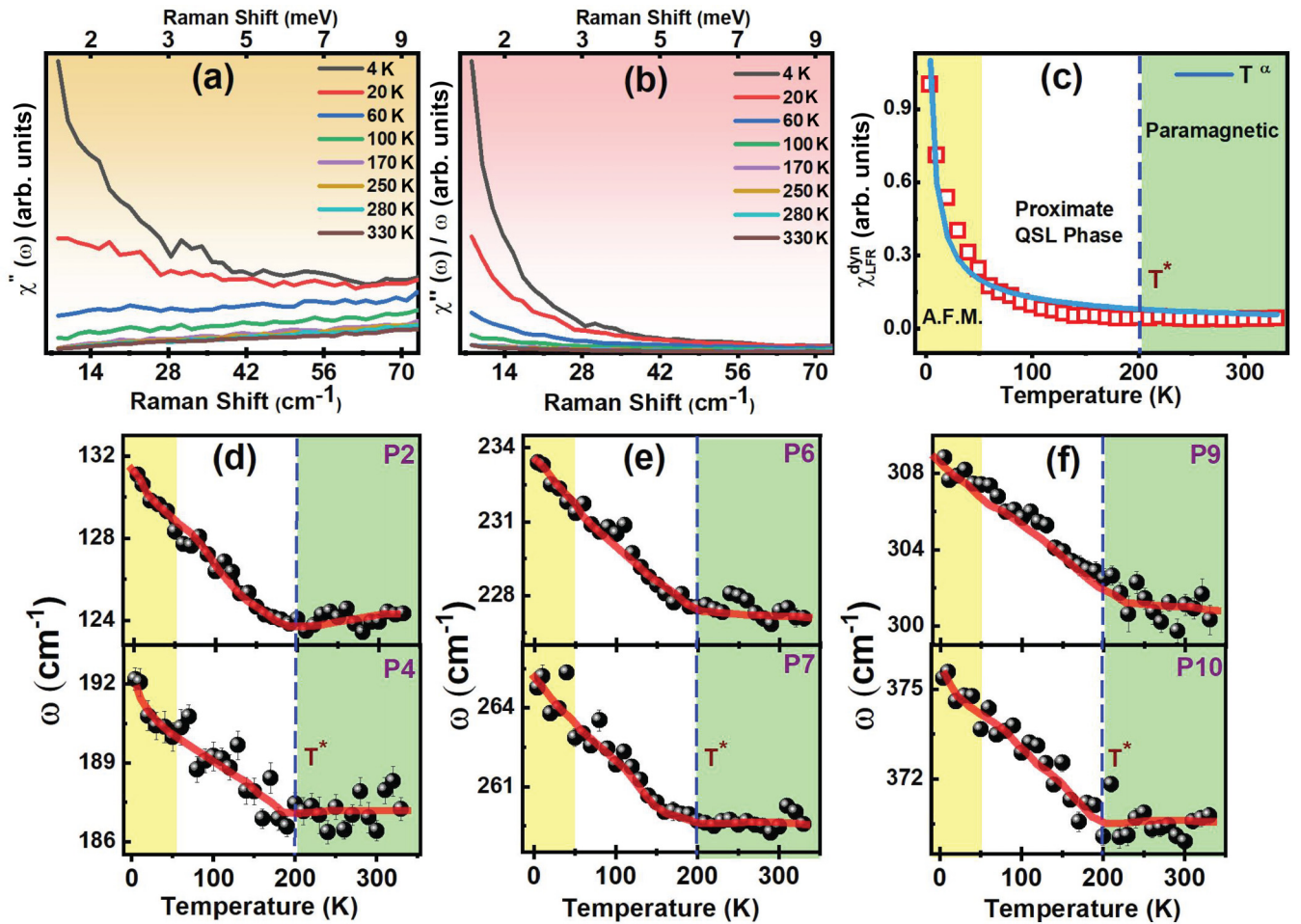


FIG. 3. (a,b) show the temperature evolution of the Bose-corrected spectra, i.e., Raman response $\chi''(\omega, T)$ and Raman conductivity $\chi''(\omega, T)/\omega$ in the low frequency region LFR (1–9.0 meV), respectively. (c) Temperature dependence of $\chi_{\text{LFR}}^{\text{dyn}}(T)$ obtained from the Kramers-Kronig relation. The solid blue line is the power-law fit $\chi_{\text{LFR}}^{\text{dyn}} \sim T^\alpha$. Background colored shading reflects different magnetic phases. (d – f) Mode frequency evolution as a function of temperature for the modes P2, P4, P6, P7, P9, and P10. Red solid lines are a guide to the eye. T^* (~ 200 K) represents the temperature where spin fractionalization starts building up.

in Fig. 3(c)). Here we observed the power-law behavior of χ^{dyn} and $\chi_{\text{LFR}}^{\text{dyn}}$ much above T_N , unlike the conventional pure paramagnetic phase where it is expected to show saturation. The power-law dependence of χ^{dyn} and $\chi_{\text{LFR}}^{\text{dyn}}$ even well above the long-range magnetic ordering temperature reflects the slowly decaying correlation inherent to the quantum spin liquid phase and triggers fractionalization of spins into itinerant fermions around $T^* \sim 200$ K [60,61]. We note that this anomalous temperature evolution of the background continuum along with phonon anomalies, discussed later, cannot be captured by the conventional long range ordered magnetic scattering; rather, it reflects the presence of fractionalized excitations which are intimately linked with the quantum spin liquid phase, in line with the theoretical suggestions for a QSL state. It may be mentioned that the underlying continuum may have its origin in the two-magnon excitations, though a detailed magnetic field dependent Raman measurement is required to further shed light on the nature of this continuum.

We wish to note that in a recent report for the case of a putative QSL candidate RuCl_3 [16], the QSL phase is

predicted with long range ordering at $T_N \sim 7$ K (zigzag AFM state). It is shown that in the high temperature the paramagnetic phase quasielastic intensity of magnetic excitation has a broad continuum and the low temperature AFM state is quite fragile with competition from FM correlation and the QSL phase; in fact, the AFM state is advocated to be stabilized by quantum fluctuations leaving the QSL and FM states as proximate to the |GS), and at a slightly higher temperature the Kitaev QSL state becomes prominent. Furthermore, it was advocated that the FM and QSL states proximate to the AFM |GS) are essential to understanding the anomalous scattering continuum. Based on our observations and phonon anomalies (discussed in the next section) this broad magnetic continuum is attributed to the fractionalized excitations in this material with a quasi-2D magnetic honeycomb lattice.

B. Mode asymmetry and anomalous phonons

Interaction of the underlying magnetic continuum with the lattice degrees of freedom may reflect via the

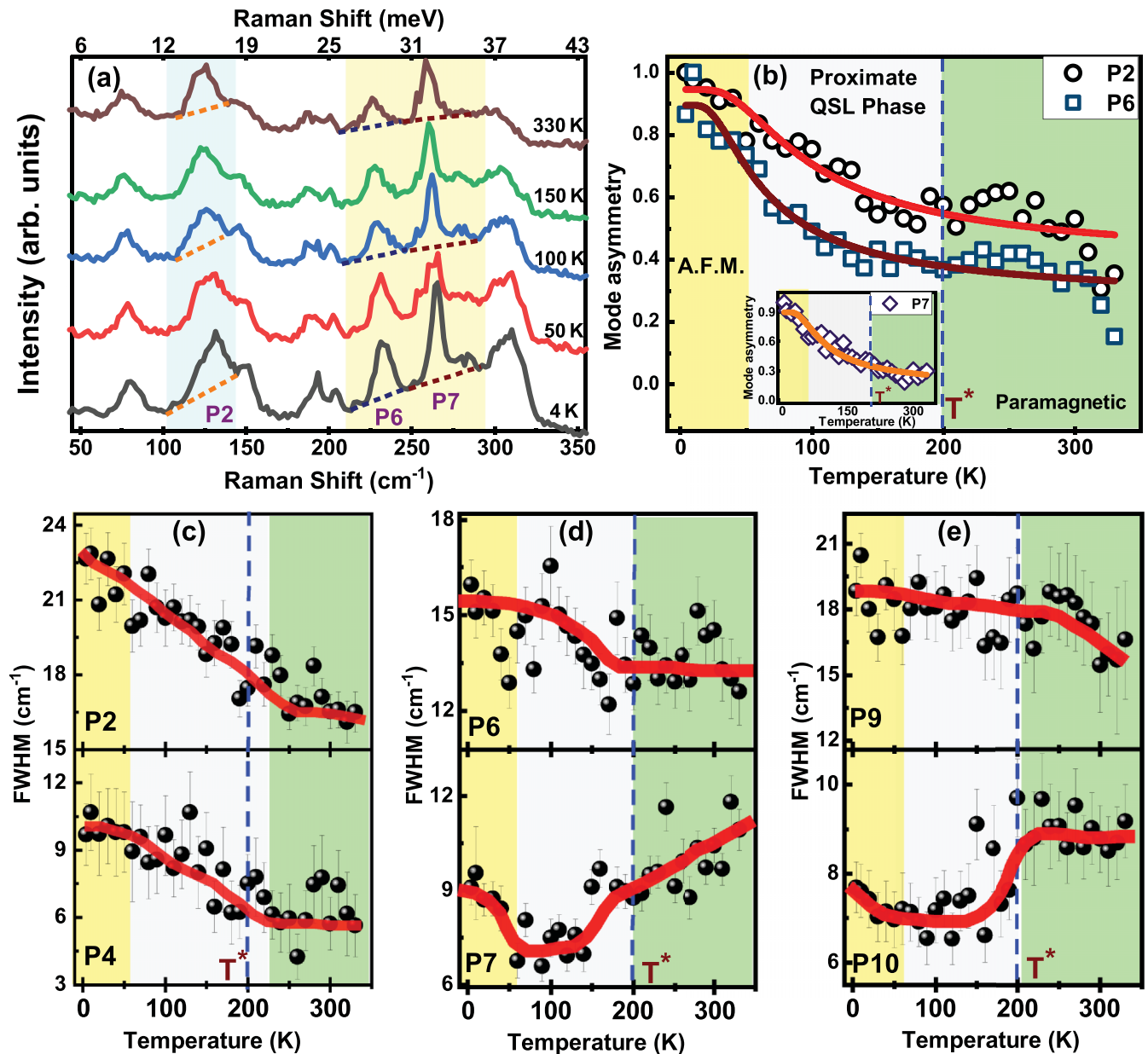


FIG. 4. (a) Shows the raw Raman spectrum in the frequency range of $\sim 45\text{--}360\text{ cm}^{-1}$ showing the evolution of the asymmetry for the modes P2, P6, and P7. (b) Shows the evolution of the phonon modes P2, P6, and P7 (as the inset) normalized asymmetry gauged via slope. Background colored shading reflects different magnetic phases. (c – e) show the linewidth for the modes P2, P4, P6, P7, P9, and P10. Red solid lines are a guide to the eye. T^* ($\sim 200\text{ K}$) represents the temperature where spin fractionalization starts building up.

asymmetric nature of the phonon line shape, known as Fano asymmetry, and may provide crucial information about the nature of the underlying magnetic excitations responsible for the magnetic continuum. This asymmetry basically describes the interaction of a continuum with a discrete state (Raman active phonon modes here) and this effect has its origin in the spin-dependent electron polarizability which involves both spin-photon and spin-phonon coupling [62–64]. For the Kitaev spin liquid candidates, recently it was advocated that spin-phonon coupling renormalizes phonon propagators and generates the Fano line shape, resulting in the observable effect of the Majorana fermions and the Z_2 gauge fluxes, a common denominator for a Kitaev quantum spin liquid

[GS] [65,66]. The evolution of phonon mode asymmetry in putative QSL candidate materials seems ubiquitous [39, 67–69], suggesting the intimate link between the QSL phase and phonon asymmetric line shape. Additionally, it was also shown that the lifetime of the phonons decreases with decreasing temperature, i.e., increase in linewidth with decreasing temperature, attributed to the decay of phonons into itinerant Majorana fermions [70]. This is opposite to the conventional behavior where the phonon linewidth decreases with decreasing temperature owing to reduced phonon-phonon interactions.

Figure 4(a) shows the temperature-dependent Raman spectra in a frequency range where a few modes (P2, P6, and

P7) show strong asymmetric line evolution. It is very clear that these phonon modes gain an asymmetric line shape with decreasing temperature. As expected, these modes are superposed on the broad underlying magnetic continuum in the region where the spectral weight of the continuum is dominating. The asymmetric nature of these three phonon modes is gauged via the slope method; see the Supplemental Material (Sec. S5) [19] for details and equivalence between the slope method and the Fano function [$F(\omega) = I_0(q + \varepsilon)^2 / (1 + \varepsilon^2)$, where $\varepsilon = (\omega - \omega_0) / \Gamma$ and $1/q$ is defined as asymmetry parameter]. Here we have adopted the slope method because the Fano function fitting resulted in a large error. Figure 4(b) shows the normalized slope for these three modes. Interestingly, the asymmetry gauged via slopes shows strong temperature dependence [see Fig. 4(b)]; it has a high value in the long range ordered phase at low temperature. Above T_N (~ 60 K) it continuously decreases until ~ 200 K, and thereafter it remains nearly constant up to 330 K, clearly suggesting the presence of active magnetic degrees of freedom far above T_N . A pronounced feature of this mode asymmetry is that it conjointly varies with dynamic Raman susceptibility on varying temperature [discussed above; see Figs. 2(c) and 3(c)], implying that its asymmetric line shape is also an indicator of spin fractionalization or the emergence of the spin liquid phase, and the increased value below 200 K (T^* is defined as a crossover temperature) may be translated to a growth of finite spin fractionalization. We also tried to fit the temperature evolution of the slopes with the two-fermion scattering form $a + b[1 - f(\omega, T)]^2$ [see Fig. 4(b)] and the extracted fermionic energy scale is also found to be similar to that estimated from intensity fitting of the continuum background [see Fig. 2(d)]. It is quite interesting that the evolution of the mode's asymmetry for these phonon modes maps parallel to the thermal damping of the fermionic excitations. In materials with the Kitaev QSL phase as [GS], spins are fractionalized into the Majorana fermions; as a result of this the underlying continuum emerging from spin fractionalization couples strongly with lattice degrees

of freedom as evidenced here. The temperature evolution of these modes, i.e., the phonon mode's line asymmetry, in line with the theoretical prediction, suggests the fractionalization of spins.

For a normal phonon mode behavior, as the temperature is lowered then the phonon peak energy is increased and the linewidth decreases, attributed to the anharmonic phonon-phonon interactions. Interestingly, a large number of modes showed a change in phonon frequency at the crossover temperature T^* (~ 200 K), signaling the effect of spin fractionalization on the phonon modes; see Figs. 3(d)–3(f). Startlingly, some of the modes showed anomalous evolution of the linewidth below T^* ; i.e., the linewidth increases with decreasing temperature. Figures 4(c)–4(e) show the temperature dependence of the linewidth of the phonon modes which show anomalous behavior. All these modes show clear divergence from the normal behavior starting at the crossover temperature T^* , implying an additional decay channel, similar to the temperature scale associated with the phonon mode's line asymmetry and magnetic continuum reflected via dynamic Raman susceptibility. This is also consistent with the theoretical predictions; hence our observation clearly evidenced the emergence of fractionalized excitations in this quasi-2D magnetic system starting from the crossover temperature reflected via phonon anomalies and broad underlying magnetic continuum.

III. CONCLUSION

In conclusion, we have performed in-depth inelastic light scattering (Raman) studies on $V_{1-x}PS_3$ single crystals, where we focused on the background continuum showing distinct temperature dependence via dynamic Raman susceptibility and the phonons' anomalies. Our results on background continuum and phonon self-energy parameters evince an anomaly at a similar temperature range, suggesting the crossover from a normal paramagnetic phase to a state where spin fractionalization begins and also marks the onset of proximate

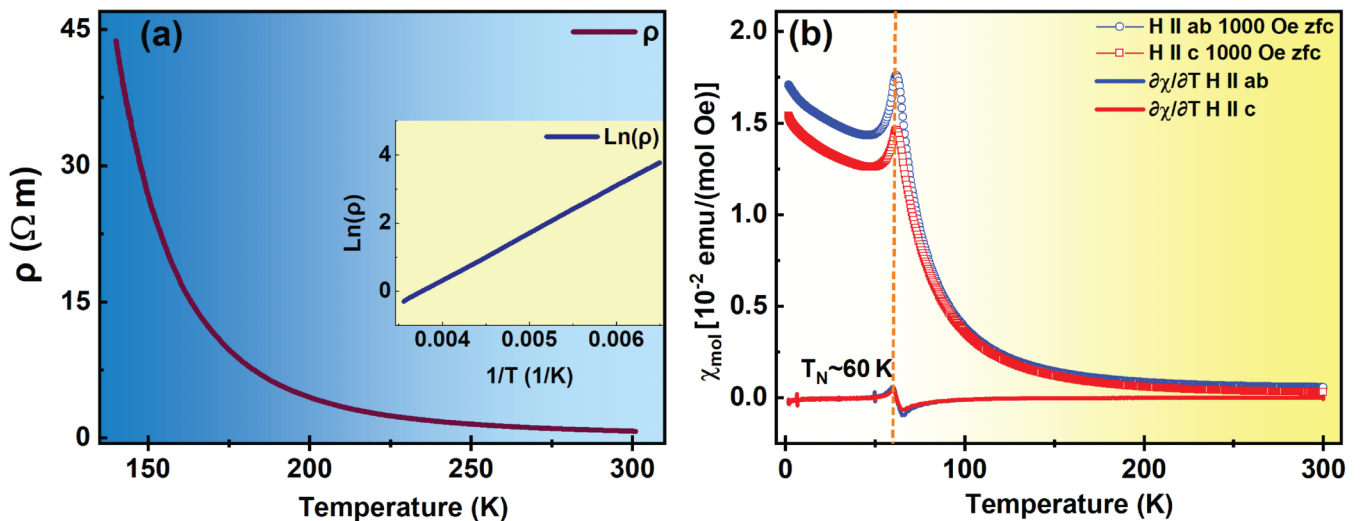


FIG. 5. (a) Resistivity as a function of temperature; inset shows $\ln(\rho)$ vs $1/T$. (b) Molar magnetic susceptibility χ_{mol} in ZFC mode with $H \parallel ab$ plane and $H \parallel c$ axis along with the respective derivatives.

TABLE I. Wyckoff positions of different atoms in conventional unit cell and irreducible representations of the phonon modes of monoclinic $\{C2/m[C_{2h}]\}V_{1-x}PS_3$ at the gamma point. R_{A_g} and R_{B_g} are the Raman tensors for the A_g and B_g phonon modes.

Atoms	Wyckoff site	Γ -point mode decomposition	Raman tensor
V	4g	$A_g + A_u + 2B_g + 2B_u$	$R_{A_g} = \begin{pmatrix} a & 0 & d \\ 0 & b & 0 \\ d & 0 & c \end{pmatrix}$
P	4i	$2A_g + A_u + B_g + 2B_u$	$R_{B_g} = \begin{pmatrix} 0 & e & 0 \\ e & 0 & f \\ 0 & f & 0 \end{pmatrix}$
S	4i	$2A_g + A_u + B_g + 2B_u$	
S	8j $\Gamma_{\text{Raman}} = 8A_g + 7B_g$	$3A_g + 3A_u + 3B_g + 3B_u$ $\Gamma_{\text{Infrared}} = 6A_u + 9B_u$	

quantum spin liquid phase. Our studies evinced the signature of spin fractionalization in this quasi-2D magnetic honeycomb lattice system. In addition to the observation of a broad magnetic continuum and its anomalous temperature evolution, our results on the evolution of the modes' line asymmetry and phonon anomalies, in particular for the phonon modes lying on the underlying magnetic continuum, opens the possibility to experimentally identify the theoretically predicted effects of fractionalized excitations of the QSL phase in putative spin liquid candidates.

ACKNOWLEDGMENTS

P.K. thanks IIT Mandi and the Department of Science and Technology-India for the financial support. S.A. acknowledges the support of Deutsche Forschungsgemeinschaft

(DFG) through Grant No. AS 523/4-1. B.B. acknowledges financial support from the DFG through the Würzburg-Dresden Cluster of Excellence on Complexity and Topology in Quantum Matter-ct.qmat (EXC 2147, Project No. 390858490).

APPENDIX

1. Resistivity and magnetization measurements

Figure 5(a) shows the resistivity vs T plot. The inset shows the log of resistivity as a function of temperature; an Arrhenius fitting gives the band gap of ~ 180 meV. Magnetic susceptibility measurement was performed in the zero field cooling (ZFC) mode at $H_{\text{ex}} = 1000$ Oe shown in Fig. 5(b) which shows $T_N \sim 60$ K, respectively, is very close to $T_N \sim 62$ K which was reported by Coak *et al.* [1]. Magnetic susceptibility increases slowly as temperature is decreased from 300 K

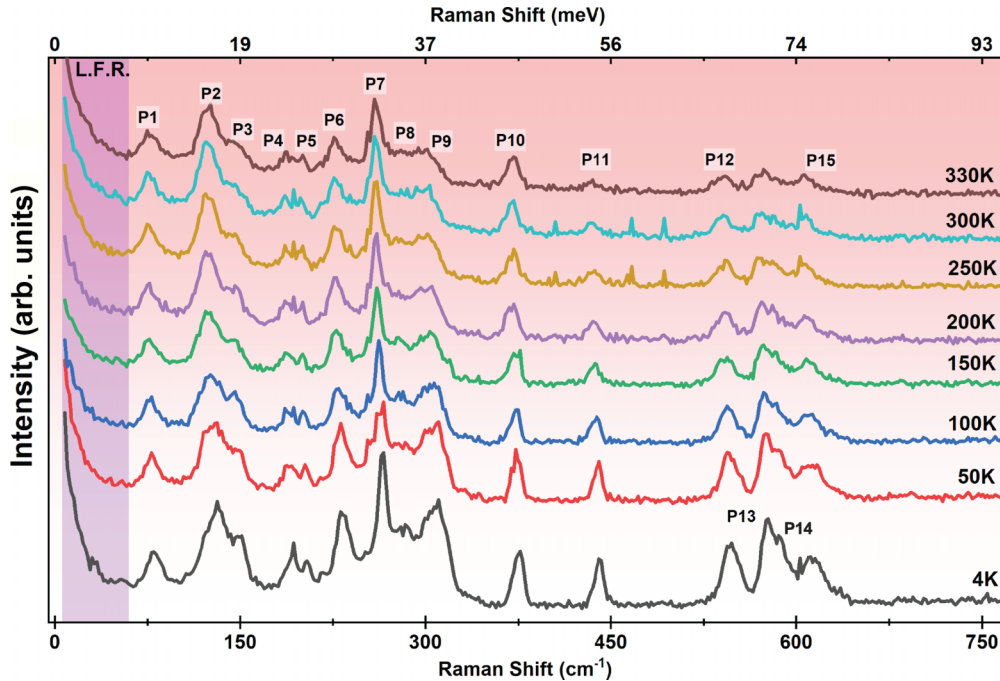


FIG. 6. Raw spectra of bulk $V_{0.85}PS_3$ along with peak labels at different temperatures within the spectral range of $5\text{--}760\text{ cm}^{-1}$. Low frequency region (LFR) is shaded in purple.

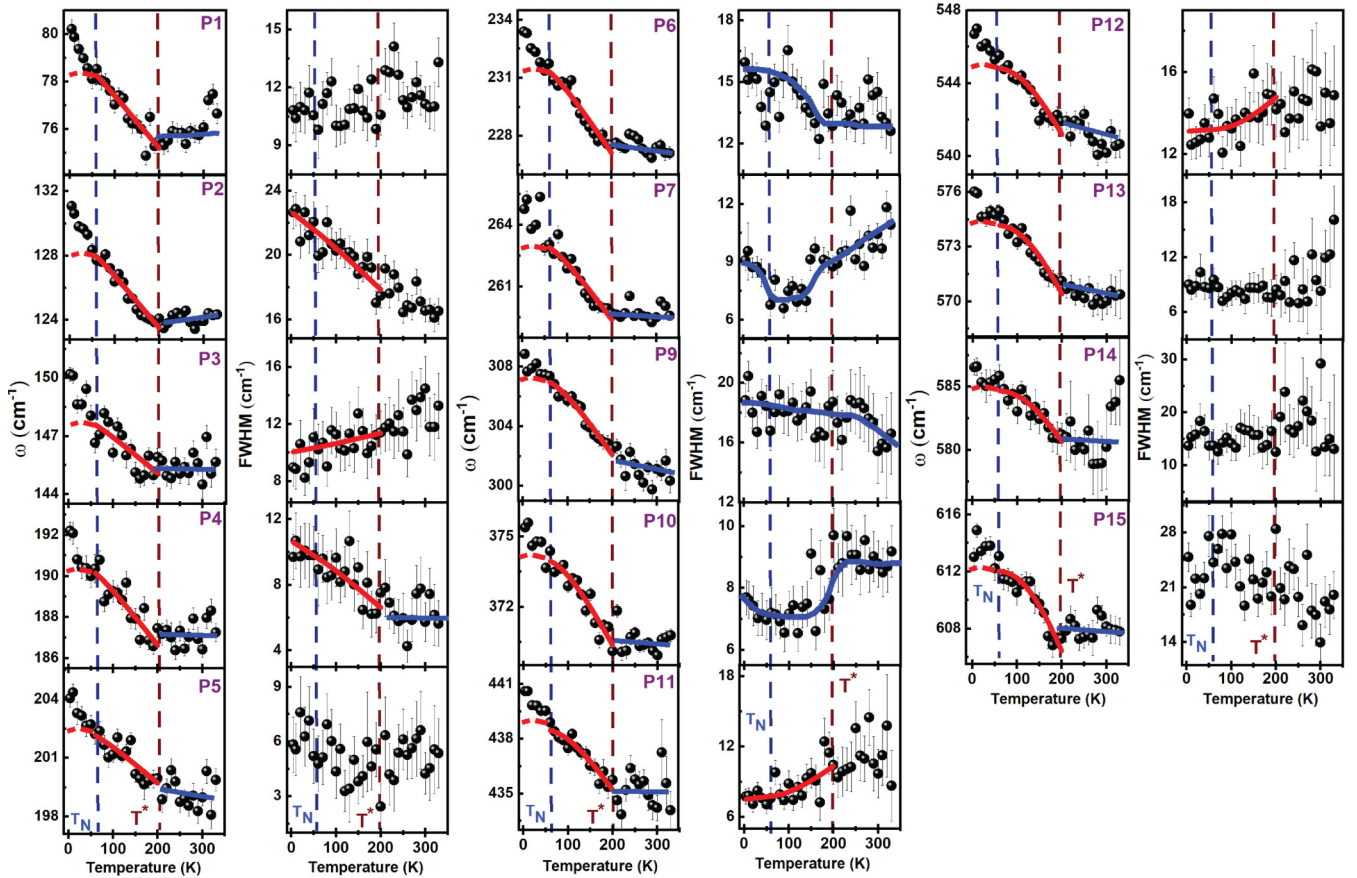


FIG. 7. Temperature-dependent evolution of features (frequency and FWHM) of the phonon modes. Some of the phonons were fitted with the anharmonic model as mentioned in the text indicated by solid red and blue lines which are a guide to the eye. Dotted vertical lines represent T_N (~ 60 K) and crossover temperature T^* (~ 200 K).

and shows a sharp decrease around 60 K. In the paramagnetic phase it shows no deviation, but once the spin-solid phase is reached the magnetic susceptibility starts to show anisotropic behavior, which suggests that it is comparatively easier to magnetize the sample in the ab plane than along the c axis. Interestingly below ~ 50 K, susceptibility again starts increasing, which is very unlikely in the case of conventional antiferromagnets where net magnetization goes to zero sharply below the Néel temperature. For Fe, Mn, and Ni, χ_{mol} vs T showed behavior of a typical antiferromagnetic (AFM) system; i.e., $\chi_{\text{mol}}^{\parallel}$ parallel to the magnetization axis shows a sharp drop below T_N , whereas $\chi_{\text{mol}}^{\perp}$ perpendicular to the magnetic axis remains nearly constant with a slight increase owing to the presence of spin waves [2,4,71]. Surprisingly in the case of $V_{1-x}PS_3$ both $\chi_{\text{mol}}^{\parallel}$ and $\chi_{\text{mol}}^{\perp}$ show similar (increases with decrease in temperature) behavior below T_N unlike that of a typical AFM system. Such a complex magnetic behavior could be a reflection of a quantum spin disordered state. Increase in $\chi_{\text{mol}}^{\parallel}$ and $\chi_{\text{mol}}^{\perp}$ below T_N reflects the dominance of only short-range ordering. This can be a signal of a proximate QSL state or may be a remnant of a QSL state existing as a fluctuation even within the spin-solid phase. We note that similar behavior of χ_{mol} below T_N was also reported for $\text{Cu}_2\text{Te}_2\text{O}_5\text{Br}_2$ [6,7], which could be understood

by a quantum critical transition from the AFM state to the QSL state.

We also extracted the net effective moments by fitting the inverse magnetic susceptibility data using a modified Curie-Weiss law in the temperature range of 200–300 K with linear extrapolation below 200 K; the extracted value of the effective magnetic moment is $\mu_{\text{eff}}^{\text{expt.}} = 3.61\mu_B$ and $\mu_{\text{eff}}^{\text{expt.}} = 3.68\mu_B$ for in-plane (H parallel to the ab plane) and out of plane (H parallel to c axis) measurements, respectively. The theoretical value of the effective magnetic moment for V^{3+} ($S = 1$) is $\mu_{S=1} = 2.83\mu_B$, for V^{2+} ($S = \frac{3}{2}$) it is $\mu_{S=\frac{3}{2}} = 3.87\mu_B$, and for the average spin $\mu_{S=1.32} = 3.50\mu_B$. We found the experimental value of $\mu_{\text{eff}}^{\text{expt.}} = 3.61\mu_B$ which is within $\sim 4\%$ error of the theoretically estimated value using average spin.

2. Temperature-dependent phonon analysis

In the stoichiometric structure of VPS_3 , the factor group analysis predicts a total of 30 nondegenerate modes, $\Gamma = 8A_g + 7B_g + 6A_u + 9B_u$, within the irreducible representation at the gamma point, out of which 15, $\Gamma_{\text{Raman}} = 8A_g + 7B_g$, are Raman active with symmetric A_g and antisymmetric B_g lattice vibrations, and 15, $\Gamma_{\text{infrared}} = 6A_u + 9B_u$, are infrared in nature; details are summarized in Table I. Figure 6

TABLE II. Anharmonic fitting parameters of the phonon modes and symmetry assignment.

Modes (symmetry)	ω_o	A	Γ_o	C
P1(B_g)	79.7 \pm 0.4	-00.6 \pm 0.1		
P2(B_g)	130.4 \pm 0.4	-01.6 \pm 0.1	23.3 \pm 0.7	-1.2 \pm 0.2
P3(B_g)	149.1 \pm 0.7	-01.1 \pm 0.2	09.8 \pm 1.1	0.4 \pm 1.4
P4(B_g)	192.5 \pm 0.7	-01.9 \pm 0.3	11.7 \pm 1.1	-1.7 \pm 0.5
P5(B_g)	203.9 \pm 0.5	-01.5 \pm 0.2		
P6(A_g)	234.7 \pm 0.4	-03.1 \pm 0.2		
P7(A_g)	266.2 \pm 0.4	-03.0 \pm 0.2		
P9(A_g)	312.5 \pm 0.5	-05.3 \pm 0.4		
P10(A_g)	379.5 \pm 0.6	-05.4 \pm 0.5		
P11(B_g)	445.1 \pm 0.8	-06.6 \pm 0.7	02.5 \pm 2.3	5.2 \pm 2.0
P12(A_g)	556.0 \pm 1.5	-11.7 \pm 1.4	08.0 \pm 2.8	5.1 \pm 2.6
P13(B_g)	588.0 \pm 1.6	-13.9 \pm 1.5		
P14(A_g)	600.1 \pm 2.5	-15.4 \pm 2.3		
P15(A_g)	637.1 \pm 3.1	-25.0 \pm 2.9		

shows the evolution of the Raman spectra with temperature. We found 15 modes, which is consistent with group theory prediction as well. We have fitted the Raman spectra at different temperatures with the Lorentzian function and extracted corresponding phonon self-energy parameters.

The effect of the thermal part of anharmonicity can be visualized in temperature-dependent variation of phonon frequencies and linewidth in the three-phonon process using the following functional forms [72]:

$$\omega(T) = \omega_o + A \left(1 + \frac{2}{e^x - 1} \right), \quad (\text{A1})$$

$$\Gamma(T) = \Gamma_o + C \left(1 + \frac{2}{e^x - 1} \right), \quad (\text{A2})$$

respectively; here ω_o and Γ_o are frequency and linewidth at absolute zero; $x = \frac{\hbar\omega_o}{2k_B T}$, $y = \frac{\hbar\omega_o}{3k_B T}$, A , and C are the self-energy constants [73]. The three-phonon contribution is fitted and shown by the thick red curve in Fig. 7 in a temperature range of 60–200 K for temperature-dependent frequency and linewidth of P1–P7, P9–P15 modes; the estimated deviation from a cubic anharmonic model below 60 K is indicated by an extrapolated dashed red curve. This extrapolated curve below 60 K is based on the constant parameter obtained by fitting in the range of 60–200 K. We obtained a negative value of “ A ” for all the modes which implies phonon display blueshift with decreasing temperature, which is considered as normal behavior when fitted using the cubic anharmonic model; derived parameters are summed up in Table II. We clearly spot the deviation from the three-phonon process as the phonon modes blueshift below the transition temperature, which can be attributed to the interaction of magnetic and lattice degrees of freedom. Interestingly, above 200 K we observe temperature-independent behavior for most of the phonon modes. We observed that the P1–P9 phonon modes reside on that part of the spectra where there is a significant effect of the background continuum beyond which it loses intensity and temperature dependence considerably. In fact, it peaks around the P6 and P7 modes. In Fig. 8 we have shown variation of phonon self-energy parameter A with increasing phonon frequencies. A slow but gradual linear increase in

A is observed for P1 – P9 and it increases drastically for P10–P15.

For variation in full width at half maximum (FWHM), the self-energy constant “ C ” is expected to be positive as the phonon population decreases with a decrease in temperature which increases the phonon lifetime; we observe it for the modes P3, P11, and P12, whereas P2, P4, and P6 show the opposite behavior. Interestingly P13 and P14 below 200 K remain almost constant until 4 K which is anomalous behavior. P2 and P4 show significant increase in FWHM below 200 K. The linewidth of the mode P10 shows quite interesting behavior; below 200 K it shows a sharp drop and remains nearly constant until \sim 60 K and below 60 K it starts increasing. Similarly, the linewidth of mode P7 shows a drop around 200 K and then remains constant until \sim 60 K; at lower temperature it starts increasing. The different extent of variation of FWHM for different phonon modes suggest that underlying magnetic degrees of freedom are interacting in a different fashion with different energy phonon modes.

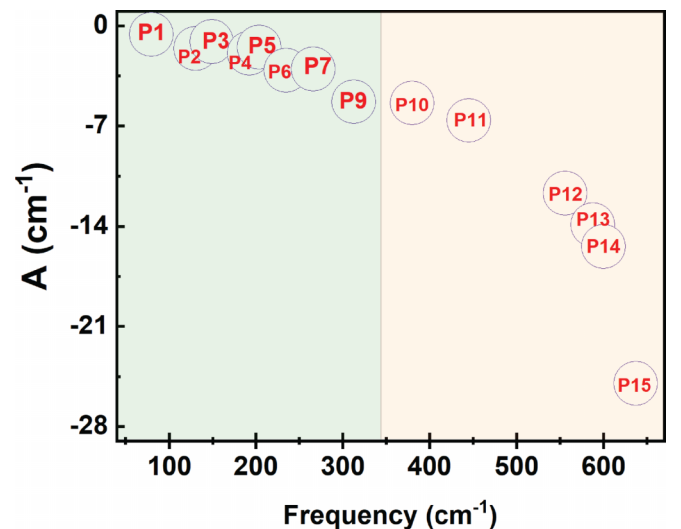


FIG. 8. Variation of the phonon self-energy parameter A with phonon frequencies.

- [1] M. J. Coak, S. Son, D. Daisenberger, H. Hamidov, C. R. S. Haines, P. L. Alireza, A. R. Wildes, C. Liu, S. S. Saxena, and J.-G. Park, *npj Quantum Mater.* **4**, 38 (2019).
- [2] X. Wang, K. Du, Y. Y. F. Liu, P. Hu, J. Zhang, Q. Zhang, M. H. S. Owen, X. Lu, C. K. Gan, P. Sengupta, C. Kloc, and Q. Xiong, *2D Mater.* **3**, 031009 (2016).
- [3] J. U. Lee, S. Lee, J. H. Ryoo, S. Kang, T. Y. Kim, P. Kim, C. H. Park, J. G. Park, and H. Cheong, *Nano Lett.* **16**, 7433 (2016).
- [4] P. A. Joy and S. Vasudevan, *Phys. Rev. B* **46**, 5425 (1992).
- [5] R. Wang, Y. Wang, Y. X. Zhao, and B. Wang, *Phys. Rev. Lett.* **127**, 237202 (2021).
- [6] P. Lemmens, G. Güntherodt, and C. Gros, *Phys. Rep.* **375**, 1 (2003).
- [7] A. V. Sologubenko, R. Dell'Amore, H. R. Ott, and P. Millet, *Eur. Phys. J. B* **42**, 549 (2004).
- [8] A. Kitaev, *Ann. Phys.* **321**, 2 (2006).
- [9] G. Jackeli and G. Khaliullin, *Phys. Rev. Lett.* **102**, 017205 (2009).
- [10] S. K. Choi, R. Coldea, A. N. Kolmogorov, T. Lancaster, I. I. Mazin, S. J. Blundell, P. G. Radaelli, Y. Singh, P. Gegenwart, K. R. Choi, S. W. Cheong, P. J. Baker, C. Stock, and J. Taylor, *Phys. Rev. Lett.* **108**, 127204 (2012).
- [11] X. Liu, T. Berlijn, W. G. Yin, W. Ku, A. Tsvelik, Y.-J. Kim, H. Gretarsson, Y. Singh, P. Gegenwart, and J. P. Hill, *Phys. Rev. B* **83**, 220403(R) (2011).
- [12] K. W. Plumb, J. P. Clancy, L. J. Sandilands, V. V. Shankar, Y. F. Hu, K. S. Burch, H.-Y. Kee, and Y.-J. Kim, *Phys. Rev. B* **90**, 041112(R) (2014).
- [13] C. Xu, J. Feng, H. Xiang, and L. Bellaiche, *npj Comput. Mater.* **4**, 57 (2018).
- [14] C. Xu, J. Feng, M. Kawamura, Y. Yamaji, Y. Nahas, S. Prokhorenko, Y. Qi, H. Xiang, and L. Bellaiche, *Phys. Rev. Lett.* **124**, 087205 (2020).
- [15] M. Saito, R. Takagishi, N. Kurita, M. Watanabe, H. Tanaka, R. Nomura, Y. Fukumoto, K. Ikeuchi, and R. Kajimoto, *Phys. Rev. B* **105**, 064424 (2022).
- [16] H. Suzuki, H. Liu, J. Bertinshaw, K. Ueda, H. Kim, S. Laha, D. Weber, Z. Yang, L. Wang, H. Takahashi, K. Fürsich, M. Minola, B. V. Lotsch, B. J. Kim, H. Yavaş, M. Daghofer, J. Chaloupka, G. Khaliullin, H. Gretarsson, and B. Keimer, *Nat. Commun.* **12**, 4512 (2021).
- [17] Y. S. Choi, C. H. Lee, S. Lee, S. Yoon, W. J. Lee, J. Park, A. Ali, Y. Singh, J.-C. Orain, G. Kim, J.-S. Rhyee, W.-T. Chen, F. Chou, and K.-Y. Choi, *Phys. Rev. Lett.* **122**, 167202 (2019).
- [18] S.-H. Do, C. H. Lee, T. Kihara, Y. S. Choi, S. Yoon, K. Kim, H. Cheong, W.-T. Chen, F. Chou, H. Nojiri, and K.-Y. Choi, *Phys. Rev. Lett.* **124**, 047204 (2020).
- [19] See Supplemental Material at <http://link.aps.org/supplemental/10.1103/PhysRevB.107.094417> for discussions about the experimental techniques, and temperature and polarization analysis of the phonons; this includes Refs. [1,20–33].
- [20] Y. Shemerliuk, Y. Zhou, Z. Yang, G. Cao, A. U. B. Wolter, B. Büchner, and S. Aswartham, *Electron. Mater.* **2**, 284 (2021).
- [21] S. Selter, Y. Shemerliuk, M. I. Sturza, A. U. B. Wolter, B. Büchner, and S. Aswartham, *Phys. Rev. Mater.* **5**, 073401 (2021).
- [22] S. Selter, Y. Shemerliuk, B. Büchner, and S. Aswartham, *Crystals* **11**, 500 (2021).
- [23] F. Bougamha, S. Selter, Y. Shemerliuk, S. Aswartham, A. Benali, B. Büchner, H.-J. Grafe, and A. P. Dioguardi, *Phys. Rev. B* **105**, 024410 (2022).
- [24] A. P. Dioguardi, S. Selter, U. Peeck, S. Aswartham, M. I. Sturza, R. Murugesan, M. S. Eldeeb, L. Hozoi, B. Büchner, and H. J. Grafe, *Phys. Rev. B* **102**, 064429 (2020).
- [25] S. Spachmann, A. Elghandour, S. Selter, B. Büchner, S. Aswartham, and R. Klingeler, *Phys. Rev. Res.* **4**, L022040 (2022).
- [26] R. F. G. Ouyard, R. Brec, and J. Rouxel, *Mater. Res. Bull.* **20**, 1053 (1985).
- [27] W. Klingen, G. Eulenberger, and H. Hahn, *Z. Anorg. Allg. Chem.* **401**, 97 (1973).
- [28] A. J. Martinolich, S. D. Ware, B. C. Lee, and K. A. See, *J Phys.: Mater.* **4**, 024005 (2021).
- [29] A. H. Larsen, J. J. Mortensen, J. Blomqvist, I. E. Castelli, R. Christensen, M. Dułak, J. Friis, M. N. Groves, B. Hammer, C. Hargus, E. D. Hermes, P. C. Jennings, P. B. Jensen, J. Kermode, J. R. Kitchin, E. Leonhard Kolsbjerg, J. Kubal, K. Kaasbjerg, S. Lysgaard, J. B. Maronsson *et al.*, *J. Condens. Matter Phys.* **29**, 273002 (2017).
- [30] B. Singh, M. Vogl, S. Wurmehl, S. Aswartham, B. Büchner, and P. Kumar, *Phys. Rev. Res.* **2**, 043179 (2020).
- [31] D. Kumar, B. Singh, R. Kumar, M. Kumar, and P. Kumar, *J. Phys.: Condens. Matter* **32**, 415702 (2020).
- [32] R. Loudon, *Adv. Phys.* **13**, 423 (1964).
- [33] F. A. Cotton, *Chemical Applications of Group Theory* (Wiley-Interscience, New York, 1990).
- [34] S. Yoon, M. Rübhausen, S. L. Cooper, K. H. Kim, and S. W. Cheong, *Phys. Rev. Lett.* **85**, 3297 (2000).
- [35] H. Yamase and R. Zeyher, *Phys. Rev. B* **88**, 125120 (2013).
- [36] N. Nagaosa and P. Lee, *Phys. Rev. B* **43**, 1233 (1991).
- [37] B. S. Shastry and B. I. Shraiman, *Phys. Rev. Lett.* **65**, 1068 (1990).
- [38] T. P. Devereaux and R. Hackl, *Rev. Mod. Phys.* **79**, 175 (2007).
- [39] L. J. Sandilands, Y. Tian, K. W. Plumb, Y.-J. Kim, and K. S. Burch, *Phys. Rev. Lett.* **114**, 147201 (2015).
- [40] A. Glamazda, P. Lemmens, S. H. Do, Y. S. Kwon, and K. Y. Choi, *Phys. Rev. B* **95**, 174429 (2017).
- [41] A. Glamazda, P. Lemmens, S. H. Do, Y. S. Choi, and K. Y. Choi, *Nat. Commun.* **7**, 12286 (2016).
- [42] Y. Li, A. Pustogow, M. Bories, P. Pupal, C. Krellner, M. Dressel, and R. Valentí, *Phys. Rev. B* **101**, 161115(R) (2020).
- [43] A. B. Sushkov, G. S. Jenkins, T.-H. Han, Y. S. Lee, and H. D. Drew, *J. Phys.: Condens. Matter* **29**, 095802 (2017).
- [44] D. V. Pilon, C. H. Lui, T. H. Han, D. Shrekenhamer, A. J. Frenzel, W. J. Padilla, Y. S. Lee, and N. Gedik, *Phys. Rev. Lett.* **111**, 127401 (2013).
- [45] Y. Fu, M. L. Lin, L. Wang, Q. Liu, L. Huang, W. Jiang, Z. Hao, C. Liu, H. Zhang, X. Shi, J. Zhang, J. Dai, D. Yu, F. Ye, P. A. Lee, P. H. Tan, and J. W. Mei, *Nat. Commun.* **12**, 3048 (2021).
- [46] N. Hassan, S. Cunningham, E. I. Zhilyaeva, S. A. Torunova, R. N. Lyubovskaya, J. A. Schlueter, and N. Drichko, *Crystals* **8**, 233 (2018).
- [47] N. Drichko, R. Hackl, and J. A. Schlueter, *Phys. Rev. B* **92**, 161112(R) (2015).
- [48] A. Pustogow, Y. Saito, E. Zhukova, B. Gorshunov, R. Kato, T. H. Lee, S. Fratini, V. Dobrosavljević, and M. Dressel, *Phys. Rev. Lett.* **121**, 056402 (2018).

- [49] Y. Yamaji, T. J. Suzuki, and M. Kawamura, [arXiv:1802.02854](#).
- [50] J. Knolle, G.-W. Chern, D. L. Kovrizhin, R. Moessner, and N. B. Perkins, *Phys. Rev. Lett.* **113**, 187201 (2014).
- [51] B. Perreault, J. Knolle, N. B. Perkins, and F. J. Burnell, *Phys. Rev. B* **92**, 094439 (2015).
- [52] I. Rousochatzakis, S. Kourtis, J. Knolle, R. Moessner, and N. B. Perkins, *Phys. Rev. B* **100**, 045117 (2019).
- [53] J. Nasu, J. Knolle, D. L. Kovrizhin, Y. Motome, and R. Moessner, *Nat. Phys.* **12**, 912 (2016).
- [54] B. Singh, D. Kumar, V. Kumar, M. Vogl, S. Wurmehl, S. Aswartham, B. Büchner, and P. Kumar, *Phys. Rev. B* **104**, 134402 (2021).
- [55] K. Y. Choi, P. Lemmens, D. Heydhausen, G. Güntherodt, C. Baumann, R. Klingeler, P. Reutler, and B. Büchner, *Phys. Rev. B* **77**, 064415 (2008).
- [56] T. Sekine, M. Jouanne, C. Julien, and M. Balkanski, *Phys. Rev. B* **42**, 8382 (1990).
- [57] F. Kretschmar, T. Böhm, U. Karahasanović, B. Muschler, A. Baum, D. Jost, J. Schmalian, S. Caprara, M. Grilli, C. Di Castro, J. G. Analytis, J. H. Chu, I. R. Fisher, and R. Hackl, *Nat. Phys.* **12**, 560 (2016).
- [58] W. Hayes and R. Loudon, *Scattering of Light by Crystals* (Dover, New York, 2004).
- [59] J. Yoshitake, J. Nasu, and Y. Motome, *Phys. Rev. Lett.* **117**, 157203 (2016).
- [60] M. Hermele, Y. Ran, P. A. Lee, and X.-G. Wen, *Phys. Rev. B* **77**, 224413 (2008).
- [61] J. Nasu, M. Udagawa, and Y. Motome, *Phys. Rev. Lett.* **113**, 197205 (2014).
- [62] U. Fano, *Phys. Rev.* **124**, 1866 (1961).
- [63] N. Suzuki and H. Kamimura, *J. Phys. Soc. Jpn.* **35**, 985 (1973).
- [64] T. Moriya, *J. Phys. Soc. Jpn.* **23**, 490 (1967).
- [65] K. Feng, S. Swarup, and N. B. Perkins, *Phys. Rev. B* **105**, L121108 (2022).
- [66] A. Metavitsiadis, W. Natori, J. Knolle, and W. Brenig, *Phys. Rev. B* **105**, 165151 (2022).
- [67] D. Wulferding, Y. Choi, S.-H. Do, C. H. Lee, P. Lemmens, C. Faugeras, Y. Gallais, and K.-Y. Choi, *Nat. Commun.* **11**, 1603 (2020).
- [68] D. Lin, K. Ran, H. Zheng, J. Xu, L. Gao, J. Wen, S.-L. Yu, J.-X. Li, and X. Xi, *Phys. Rev. B* **101**, 045419 (2020).
- [69] B. Singh, M. Vogl, S. Wurmehl, S. Aswartham, B. Büchner, and P. Kumar, *Phys. Rev. Res.* **2**, 013040 (2020).
- [70] S. Pal, A. Seth, P. Sakrikar, A. Ali, S. Bhattacharjee, D. V. S. Muthu, Y. Singh, and A. K. Sood, *Phys. Rev. B* **104**, 184420 (2021).
- [71] A. McCreary, J. R. Simpson, T. T. Mai, R. D. McMichael, J. E. Douglas, N. Butch, C. Dennis, R. Valdés Aguilar, and A. R. Hight Walker, *Phys. Rev. B* **101**, 064416 (2020).
- [72] P. G. Klemens, *Phys. Rev.* **148**, 845 (1966).
- [73] M. Balkanski, R. F. Wallis, and E. Haro, *Phys. Rev. B* **28**, 1928 (1983).